Technical report; TR - 221

KNMI

PV-mixing around the tropopause in an extratropical cyclone

Michael Sigmond

Koninklijk Nederlands Meteorologisch Instituut

De Bilt, 1999

Technical report = technisch rapport; TR - 221

De Bilt, 1999

PO Box 201
3730 AE De Bilt
Wilhelminalaan 10
De Bilt
The Netherlands
Telephone + 31(0)30-220 69 11
Telefax + 31 (0)30-221 04 07

Author: Michael Sigmond (IMAU)

UDC: 551.511.2
551.510.52
551.515.1

ISSN: 0169-1708

ISBN: 90-369-2165-1

● ● ● ●

PV-MIXING AROUND THE TROPOPAUSE IN AN EXTRATROPICAL CYCLONE

Michael Sigmond

PV-MIXING AROUND THE TROPOPAUSE IN AN EXTRATROPICAL CYCLONE

Michael Sigmond

Graduation research project
Performed at
The Royal Netherlands Meteorological Institute (KNMI)
Department of Climate Research and Seismology
Division of Atmospheric Composition
De Bilt, The Netherlands

Supervisors:
Peter Siegmund (KNMI)
Geert-Jan Roelofs (IMAU)
Anastasios Kentarchos (IMAU)

July, 1999

Institute of Marine and Atmospheric Research (IMAU)
University of Utrecht
Princetonplein 5
3584 CC Utrecht
The Netherlands

Dankwoord

Met veel plezier heb ik het afgelopen jaar mijn afstudeeronderzoek op het KNMI mogen doen. Hierbij wil ik graag een aantal mensen bedanken die in meer of mindere mate hebben bijgedragen aan dit onderzoek. Allereerst dank ik Peter Siegmund, mijn directe begeleider op het KNMI, die mij heel veel geholpen heeft met vrijwel alle aspecten van dit onderzoek. Ik kon altijd bij hem langskomen met problemen die hij met veel enthousiasme probeerde op te lossen. Ik heb veel van hem geleerd over het doen van onderzoek. Ook mijn IMAU-begeleiders, Geert-Jan Roelofs en Anastasios Kentarchos wil ik bedanken voor de begeleiding van het onderzoek. Bedankt voor de tips en het doorspitten van het verslag. Bedankt ook Jojanneke Meloen, met wie ik veel heb samengewerkt. Ik wil haar bedanken voor de vele dingen die ze heeft gedaan voor dit onderzoek en het lekker kritische commentaar dat ze gegeven heeft. Rinus Scheele wil ik bedanken voor de hulp die hij me gegeven heeft met betrekking tot het trajectoriënprogramma. Zonder hem zou dit onderzoek ongetwijfeld veel langer hebben geduurd. Bedankt ook Hennie Kelder voor de mogelijkheid om in deze leuke groep af te studeren, Peter van Velthoven voor de getoonde interesse en tips en Ankie Piters voor het leveren van het GOME-plaatje. Serdal mag ik niet vergeten te bedanken omdat hij me geholpen heeft met de graphics van o.a. de poster die ik gemaakt heb voor de E.G.S.-conferentie. Alle (andere) AS-ers wil ik hartelijk danken voor de gezellige sfeer, hun hulp en interesse. Van hen wil ik Renske, Mijke en Anne Grete nog speciaal noemen en bedanken voor de gezellige lunches. Ook mijn ouders, mijn oma en mijn zusje mogen niet ontbreken in dit dankwoord; bedankt voor jullie interesse in wat ik doe. En tot slot: ode aan mijn hondstrouwe achterban in Zeist.

ABSTRACT

In this report the mixing of PV (Potential Vorticity) is studied. A new Lagrangian technique is developed to calculate PV-mixing in an extratropical cyclone. This mixing is computed from the PV along trajectories, calculated from ECMWF circulation data. Special emphasis is put on the statistical significance of the results.
PV-mixing is found to be the main process of stratosphere-troposphere exchange in the investigated extratropical cyclone. The computed field of the cross-tropopause flux is dominated by elongated patterns of statistically significant large downward and small upward fluxes. The downward fluxes mainly occur in the lower part of the considered tropopause folds. The upward fluxes are found near the entrance of the folds, in the tropopause ridges. The ratio between the area averaged upward and downward cross-tropopause fluxes decreases with increasing strength of the cyclone.
Since the largest fluxes are shown to occur in the regions with the largest wind shear, the results are expected to be reliable, at least in a qualitative sense. The position of a tropopause fold along the northwest coast of Africa is confirmed by GOME total ozone observations. The results indicate that the applied Lagrangian technique is an appropriate tool for diagnosing PV-mixing in general and stratosphere-troposphere exchange in particular.

Contents

1. Introduction

Understanding and quantifying human impact on the climate system is one of the most challenging questions in atmospheric sciences. The importance of stratosphere-troposphere exchange (STE) for understanding this impact is widely acknowledged (e.g. Holton *et al.*, 1995). The transport of specific anthropogenic emissions from the ground to the stratosphere is believed to be the main cause of stratospheric ozone depletion (WMO, 1995), whereas the increasing amount of aircraft emissions in the tropopause region could have a substantial impact on climate and the atmospheric composition (IPCC, 1999).

The global scale STE is realised by a mean meridional cell, which is called the Brewer-Dobson circulation. The cell consists of upward cross-tropopause transport in the tropics, poleward drift in the stratosphere towards the winter pole, and downward transport into the extratropical winter troposphere (Brewer, 1949; Dobson, 1956).

At smaller scales, however, STE is not dominated by mean circulations, but by synoptic scale eddy processes, such as tropopause folds associated with cut-off lows, that can lead to rapid exchange of air across the tropopause (Holton *et al.*, 1995). Therefore, apart from downward cross-tropopause transport, upward cross-tropopause transport occurs in the extratropics, which can bring anthropogenic species directly into the extratropical lower stratosphere (e.g. Hoerling *et al.*, 1993). Knowledge of the instantaneous bi-directional cross-tropopause fluxes rather than the time-mean net flux is, in the presence of a cross-tropopause gradient of a chemical species, necessary to determine the fluxes of this species across the tropopause (Gettelman and Sobel, 1998). Moreover, since the anthropogenic species are emitted non-uniformly in time and space, the knowledge of the distribution of the instantaneous cross-tropopause flux (CTF) is essential for modelling the human impact on the climate.

Many efforts have been made to determine the CTF. In these studies, Eulerian diagnostic methods have been dominant. The CTF is generally computed with one of the versions of the diagnostic formula derived by Wei (1987) (hereafter called the Wei-x formula, where x is the vertical coordinate, see below).

Hoerling *et al.* (1993) diagnosed the net global-scale CTF by applying Wei's equation to twice-daily global circulation data with a horizontal resolution of $3.75° \times 3.75°$. Siegmund *et al.* (1996) investigated the STE with a more accurate numerical method and with circulation data at higher temporal and spatial resolution. They calculated the magnitudes of the upward and downward cross-tropopause fluxes separately. They found that for an accurate estimation of the local and instantaneous CTF, the spatial and temporal resolution should be at least $1° \times 1°$ and 6 hours, respectively. To cope with practical problems of time and space differencing, a complicated numerical scheme is applied. Siegmund *et al.* (1996) as well as Gettelman and Sobel (1998) both used the Wei-p formula (where p denotes pressure) and found strong dipole structures in the computed CTF field.

Wirth and Egger (1999) examined five different methods to diagnose the CTF in a cut-off low. They found that both the Wei-p and the Wei-θ formula (where θ denotes potential temperature) are unreliable. In these formulas, the CTF is a small residual of three relatively large terms, so that small errors in the individual terms can result in a large relative error in the computed CTF. A third method examined by Wirth and Egger (1999) is the Wei-PV formula, where potential vorticity is taken as the vertical coordinate. The advantage of this method is that if the tropopause is defined as a PV-surface, the formula consists of only one term. The method therefore does not suffer from the problem of strong cancellation, provided that the PV-sources can be calculated with reasonable accuracy.

Apart from these Eulerian diagnostic methods, Wirth and Egger also examined a Lagrangian method, by starting multiple trajectories on the tropopause. The pressure difference between

the endpoint of a trajectory and the tropopause at that point is then considered as a measure for the STE in the considered time interval.

Wernli and Davies (1996) describe how their Lagrangian method can be applied for diagnosing the CTF in an extratropical cyclone. Coherent ensembles of trajectories with a period of 10 days, which cross the tropopause (defined as the 2 PVU surface, 1 PVU = 10^{-6} K m^2 kg^{-1} s^{-1}), are identified. Only a small part (5-25%) of these trajectories indicate significant STE (i.e. reside within the stratosphere (troposphere) during (at least) the first four days and within the troposphere (stratosphere) for (at least) the last four days). Although this method is an appropriate tool for studying the spatial structure of STE in an extratropical cyclone, it does not give a numerical estimate of the CTF.

In the present study a new Lagrangian technique is used to calculate STE in an extratropical cyclone, where PV-mixing is expected to be the main process. The main concept of our method is the evaluation along trajectories of the air mass flux across several PV-surfaces. Unlike in previous studies, the errors in the calculated data (to be called "noise") will be discussed.

The main goal of this study is to quantify the mixing of air masses with different values of PV in cyclonic active regions around the tropopause. A secondary goal is to quantify the noise in the computed air mass flux across the PV-surfaces. We will use this noise together with a statistical test to determine whether the computed flux is statistically significant.

In section 2 the method, input data and the trajectory model will be described. The results will be presented in section 3, discussed in section 4 and summarised in section 5.

2. Method and data

2.1 Calculation of the air mass flux across a PV-surface

2.1.1 General equation

To calculate the air mass flux across a PV-surface, Wei's (1987) general formula is used, which is given by:

$$F(\rho) = \rho J_n \left(\frac{d\eta}{dt} - \frac{\partial \eta^{tp}}{\partial t} - \vec{v} \cdot \nabla \eta^{tp} \right) \quad . \qquad (1)$$

In this formula $F(\rho)$ denotes the cross-tropopause air mass flux, where ρ *is* the density of air, η is a generalised vertical coordinate with $J_n = \partial z / \partial \eta$ and $\eta^{tp}(x,y,z)$ denotes the location of the tropopause in terms of this coordinate. All terms on the right hand side are evaluated at the tropopause. The first term on the right hand side of Eq. (1) represents the exchange between the stratosphere and troposphere due to the vertical velocity $d\eta/dt$; the second term results from the temporal movement of the tropopause; the last term is due to the variation of η along the tropopause. In the real atmosphere, the three terms generally nearly cancel. The unit of F is $kg\ m^{-2}\ s^{-1}$.
Depending on the choice of the vertical coordinate, one can obtain different versions of Eq. (1). In the present study Eq. (1) is applied with PV as the vertical coordinate and the tropopause is defined as a PV-surface. The second and third term on the right hand side of Eq. (1) then vanish. After applying the hydrostatic relation, Eq. (1) becomes:

$$F = -\frac{1}{g} \frac{\partial p}{\partial PV} \frac{dPV}{dt} \quad , \qquad (2)$$

where g is the acceleration due to gravity.

2.1.2 PV-sources

According to Eq. (2), a flux implies a material change of PV. The PV of a single air parcel can be changed by diabatic heating gradients and friction (Hoskins *et al.*, 1985). In addition, the gridbox mean PV can be changed by mixing (Shapiro, 1980). The computed data also suffer from noise, which is the error in the calculated quantities due to errors in the atmospheric dataset, the computed trajectories and the numerical method to calculate PV. In section 2.2 these PV-sources will be estimated.
In the real atmosphere, the PV of a single air parcel can only be changed by diabatic heating gradients and friction. The change of PV due to mixing is a result of the model formulation of subgrid-scale processes. A restriction of a numerical (prognostic) model is that it can not calculate the evolution of the properties of every single air parcel in the atmosphere explicitly. Instead, the quantities are calculated on a grid with a finite spatial resolution. The quantities calculated in a model are therefore gridbox mean rather than local quantities. The same applies to the PV computed along a trajectory. Therefore, in the absence of diabatic heating gradients and friction, mixing of air masses with different PV leads to a change in the gridbox mean PV, although the PV of the individual air parcels is conserved. A mathematical consideration of the PV-mixing is given in appendix A.

2.1.3 Numerical method for calculating F

To compute the right-hand side of Eq. (2), we calculate the PV and ∂p/∂PV along trajectories. An example of the PV along a trajectory is shown in Figure 1.

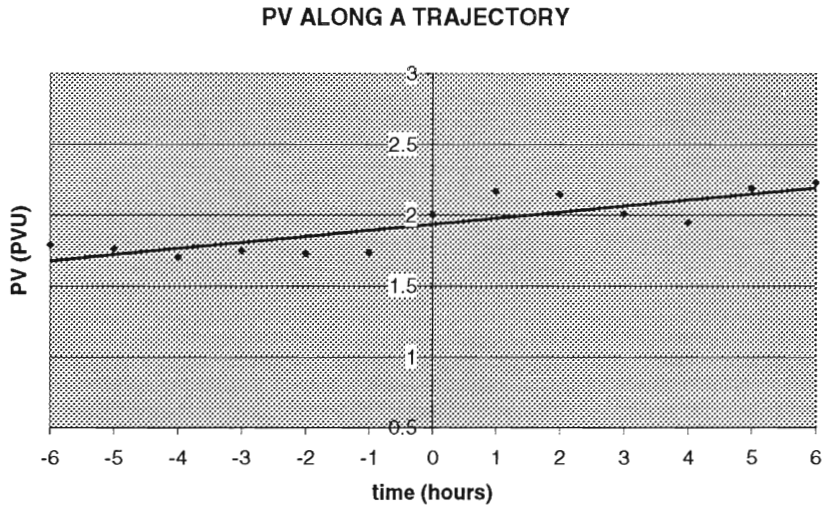

Figure 1: *Determination of the 12-hour mean dPV/dt with a linear regression of PV versus time. The trajectory model gives output data every hour.*

As can be inferred from Figure 1, the PV is partially fluctuating due to noise (the noise will be more precisely defined in section 2.2.3). The instantaneous *dPV/dt* is therefore not reliable. In order to reduce this noise, the PV should be averaged over a certain period. F is therefore approximated as:

$$\tilde{F} = -\frac{1}{g}\overline{\frac{dPV}{dt}}\ \overline{\frac{\partial p}{\partial PV}}\ , \qquad (3)$$

where

$$\overline{\frac{dPV}{dt}}$$

is the mean *dPV/dt* in the 12-h time interval obtained by a linear least square regression of the PV along the trajectory versus time, and

$$\overline{\frac{\partial p}{\partial PV}}$$

is the mean *∂p/∂PV* along the 12-h trajectory.

This flux is calculated for each gridpoint of the 3D-domain (described in section 3), by calculating PV and ∂p/∂PV along the 6-hour forward and backward trajectory that start at the gridpoint. The value of $\tilde{F}$ is then attributed to the gridpoint and the starting time of the trajectories.

2.2 Estimation of the PV-sources

In this subsection it is shown that, in the considered extratropical cyclone, the PV-change due to diabatic heating gradients and friction is small compared to the PV-change due to the mixing of PV. In addition, the method to quantify the noise is explained.

2.2.1 Friction

The PV of a single particle can only be changed by diabatic heating gradients and friction. Friction is generally neglected outside the boundary layer. Since this study deals with the fluxes near the tropopause, friction will be neglected throughout the rest of the study.

2.2.2 Estimating an upper limit of the PV-change due to diabatic heating gradients

The PV-change due to diabatic heating gradients is given by (Hoskins *et al.*, 1985):

$$\frac{dPV}{dt} = -g(\zeta + f)_\theta \frac{\partial \dot{\theta}}{\partial p} \quad , \tag{4}$$

with

$$\dot{\theta} \equiv \frac{d\theta}{dt} = \frac{Q}{c_p}\left(\frac{p_0}{p}\right)^\kappa \quad , \tag{5}$$

where θ is potential temperature, ζ is relative vorticity, f is the coriolis parameter, c_p is the specific heat of air at constant pressure, Q is the diabatic heating rate per unit mass and $\kappa = R_d/c_p$, where R_d is the gas constant for dry air.
By applying Eqs. (4) and (5) to diabatic heating fields from the NCEP reanalysis dataset (for the period '82-'94), the January mean *dPV/dt* near the tropopause at mid-latitudes is calculated. As a typical maximum value 0.05 PVU day^{-1} is found. The extremes of the instantaneous *dPV/dt* are assumed not to be more than 10 times as large as the monthly mean value, and the maximum instantaneous *dPV/dt* due to diabatic heating gradients in the tropopause region in the extratropics is therefore assumed to be not larger than about 0.5 PVU day^{-1}. This value is more than four times smaller than typical values of the *dPV/dt* from our results, as will be shown in section 3.2.1. The PV-change and thus the cross-tropopause flux due to diabatic heating gradients will therefore be neglected in this study.

2.2.3 Noise

In quantifying the noise it is assumed that during the 12h-period of the trajectories, the real PV changes linearly with time and that the real $\partial p/\partial PV$ is constant; deviation from these 'real' values are then considered as noise.
A measure for the fluctuations around a mean is the standard deviation. $\tilde{F}$ was defined as the product of a constant and the two independent quantities $\overline{dPV/dt}$ and $\overline{\partial p/\partial PV}$. The standard deviation of $\tilde{F}$ ($\sigma_{\tilde{F}}$) is therefore given by the standard deviations of $\overline{dPV/dt}$ ($\sigma_{\overline{dPV/dt}}$) and $\overline{\partial p/\partial PV}$ ($\sigma_{\overline{\partial p/\partial PV}}$) according to:

$$\left(\frac{\sigma_{\tilde{F}}}{\tilde{F}}\right)^2 = \left(\sigma_{\overline{dPV/dt}} \Big/ \overline{dPV/dt}\right)^2 + \left(\sigma_{\overline{\partial p/\partial PV}} \Big/ \overline{\partial p/\partial PV}\right)^2, \qquad (6a)$$

where

$$\sigma_{\overline{\partial p/\partial PV}} = \frac{\sigma_{\partial p/\partial PV}}{\sqrt{n}}, \qquad (6b)$$

and n is the number of data points along a trajectory (n=13). For Eq. (6b) to be valid, the different values of $\partial p/\partial PV$ along the trajectories should be independent, which is not necessarily the case. In the calculation of $\sigma_{\overline{dPV/dt}}$, on the other hand, autocorrelation of the deviations of the calculated PV-values from the linear regression line up to a time lag of 3 hours has been taken in account, applying a method described by Lyttkens (1963). The computed $\sigma_{\tilde{F}}$ is considered as the noise in $\tilde{F}$.

A Student's t-test is used to determine whether the calculated $\tilde{F}$ differs significantly from zero. The t-value is calculated as:

$$t = \frac{\overline{F}\sqrt{n-1}}{\sigma_{\tilde{F}}}, \qquad (7)$$

where $\overline{F}$ is the time mean flux along the trajectory and n=13.

The trajectory-mean flux $\overline{F}$ is given by:

$$\overline{F} = -\frac{1}{g}\left[\overline{\frac{dPV}{dt}}\;\overline{\frac{\partial p}{\partial PV}} + \overline{\left(\frac{dPV}{dt}\right)'\left(\frac{\partial p}{\partial PV}\right)'}\right], \qquad (8)$$

where the accent denotes deviations from the mean value.

In the calculation of the t-value, $\overline{F}$ is approximated by $\tilde{F}$, which implies that the eddy correlation term in Eq. (8) is neglected. In our results, $\tilde{F}$ is called statistically significant when the probability that $\tilde{F}$ differs from zero is more than 95%.

The noise in the PV along the trajectory has been investigated extensively. The quality of the trajectory model is tested with Stohl's Tracer Conservation Error (Stohl and Seibert, 1998), which measures how well PV is conserved along trajectories (not presented here). When the PV is better conserved (averaged over a large number of trajectories), the PV along a trajectory will be less noisy. From our calculations it is concluded that compared to Stohl's trajectory model our trajectory model conserves PV slightly better in the stratosphere, but slightly worse in the troposphere. Since we are considering trajectories near the tropopause, it is concluded that the quality of our trajectories is comparable to the quality of Stohl's trajectories. Further details about the noise can be found in appendix B.

2.3 Trajectory model

For calculating the trajectories, we have used the KNMI trajectory model (as described by Scheele *et al.*, 1996). This model calculates the three-dimensional displacement of air parcels for each timestep δt using the iterative scheme after Petterssen (1940). In the present study δt=10 minutes. The input circulation data are obtained from the ECMWF (see section 2.4). Spatial interpolation (linear in the horizontal and linear in the vertical with log(p)) and temporal interpolation (quadratic) are applied to the input data.

In the present study three-dimensional rather than isentropic trajectories are calculated in order to include diabatic effects in the calculations of $\tilde{F}$. Moreover, the three-dimensional trajectories are generally believed to be more accurate as is concluded, e.g., by Stohl *et al.* (1995).
For the calculation of $\tilde{F}$, the PV and the $\partial p/\partial PV$ are calculated along the trajectories. The PV is calculated as:

$$PV = -g(\zeta + f)_\theta \frac{\partial \theta}{\partial p} = -g\left[\frac{\partial \theta}{\partial p}(\zeta_p + f) + \left.\frac{\partial \theta}{\partial x}\right|_p \frac{\partial v}{\partial p} - \left.\frac{\partial \theta}{\partial y}\right|_p \frac{\partial u}{\partial p}\right] \quad , \qquad (9a)$$

with

$$\zeta_p = \left.\frac{\partial v}{\partial x}\right|_p - \frac{1}{\cos\varphi}\left.\frac{\partial (u\cos\varphi)}{\partial y}\right|_p \quad , \qquad (9b)$$

φ is the latitude, u is the zonal velocity, v is the meridional velocity and ζ is the relative vorticity. The derivatives denoted by $|_p$ are taken at constant pressure level.
To calculate the PV at place X and at time t, the PV is first calculated at the three data input times closest to time t at place X and is then quadratically interpolated to the time t.

2.4 ECMWF-data

For this study we use ECMWF circulation and temperature data of the first five days of a forecast run, which is initialised on 13 April 1998, 12 GMT. This run is performed with a spatial resolution of T213 with 31 model levels. The model data are stored every 6 hours. We use forecast data rather than analysed data in order to have a physically consistent data set, in which the modelled quantities (in particular the PV) are not disturbed by the addition of new observations. Since the difference between the +96 hour model forecast of the 500-hPa geopotential height field for 12 GMT on 17 April 1998 and the verifying analyses is very small, we assume that the forecast data give a realistic representation of the synoptic-scale processes in the considered period.

3. Results

The air mass flux across a PV-surface ($\tilde{F}$) is calculated for an extratropical cyclone over the North Sea between 14 and 17 April 1998. $\tilde{F}$ is calculated on two different 3D grids with a horizontal resolution of $1° \times 1°$: one with PV as the vertical coordinate (fluxes are calculated across the 1, 1.5, 2, 3, 4, 6, 8 and 10 PVU surfaces) and one with pressure as the vertical coordinate (from 600 hPa to 100 hPa, with a vertical resolution of 25 hPa). The horizontal domain is the area between 35°W and 25°E and between 20°N and 75°N.

3.1 Synoptic situation

The solid lines in Figure 2 show the 500-hPa geopotential height field for the period between 14 and 17 April 1998. On April 14 the cyclone has already reached maturity, on April 16 the strength of the cyclone is maximal and on April 17 the cyclone has weakened considerably. The centre of the cyclone as seen on the 500-hPa geopotential height map hardly moves; it lies at the northern part of the North Sea during the entire considered period.

3.2 Geographical distribution of the flux across PV-surfaces

3.2.1 Without significance criterion

The tropopause is generally defined as a surface of constant PV. The values mostly used vary between 1.5 and 3.5 PVU. When the tropopause is defined as the 2 PVU surface, which is an often used value, the flux across that surface is the cross-tropopause flux.
Figure 2 also shows the field of $\tilde{F}$ across the 2 PVU surface for the four different days. The field is dominated by elongated patterns of large downward and small upward fluxes. During the entire period a region with large downward fluxes far south of the cyclone centre (along the northwest coast of Africa) is visible. On April 14 (Fig. 2a), a region with large upward fluxes can be found just south of this region.
Two other regions with large downward fluxes are present on April 14: one north of the cyclone centre and one southwest of the cyclone centre, west of the 500-hPa trough. On April 15 the latter region has separated into two regions, one west and one south of the cyclone centre, in the middle of the 500-hPa trough. The region with large downward fluxes north of the centre on the 14th has moved eastward towards southeast Scandinavia. On April 16 a region with large downward fluxes is again identified southwest of the cyclone centre. Two other bands with large downward fluxes are present: the first just east of the cyclone centre, the other starting in the cyclone centre and then curling to the north. On April 17 the large downward fluxes southwest of the cyclone have vanished. The regions with large downward fluxes occur near the cyclone centre and just south of it.
The flux across the PV-surfaces decreases with increasing PV. The $\partial p/\partial PV$-field and thus the $\tilde{F}$-field across PV-surfaces lower than 2 PVU is very noisy (not shown).

In order to gain understanding of the structures in the $\tilde{F}$-field, $\tilde{F}$ across the 2 PVU surface on 14 April is decomposed in dPV/dt (Figure 3a) and $\partial p/\partial PV$ (Figure 3b). Typical values of dPV/dt are found to be in the order of $2.5 * 10^{-5}$ PVU s^{-1} (≈ 2.2 PVU day^{-1}), which is more than four times as large as the estimation of the upper limit of the PV-change due to diabatic heating gradients in an extratropical cyclone. The neglect of dPV/dt due to diabatic heating gradients therefore seems justified.

After comparing Fig. 3a and Fig. 3b with Fig. 2a, one can conclude that a condition for large (downward) fluxes is a large $\partial p/\partial PV$. A large dPV/dt does not imply a large flux when $\partial p/\partial PV$ is small. In the southwestern part of Iceland, for example, a large dPV/dt but a small $\partial p/\partial PV$ is present, which results in a small flux. When $\partial p/\partial PV$ is small, the vertical distance between the different PV-surfaces is small so that a large PV-change does not imply that much air has crossed a PV-surface.
The $\partial p/\partial PV$-field at the 2 PVU surface appears to be directly coupled to the pressure field at this surface (Fig. 3c), which is a measure for the tropopause height. The $\partial p/\partial PV$ and thus the flux is large in the areas where the tropopause pressure gradient is large (i.e. where the tropopause slopes) and in small-scale areas where the tropopause pressure itself is high (i.e. where the tropopause height is small), which can be understood from Figure 4. These conditions are valid in the tropopause folds and at the edge of a more extended lowering of the tropopause in the centre of a cyclone.

3.2.2 With significance criterion

Figure 5 shows $\tilde{F}$ across the 2 PVU surface on 14 April at 12 GMT with significance criterion, as described in section (2.2.3). Although the three areas with large downward fluxes can still be identified, it is clear that in large parts of these areas the computed fluxes are not significant.
This can be understood as follows. In a tropopause fold the values of $\partial p/\partial PV$ are relatively large. Generally they are negative, but in certain parts of the fold they can be positive. As a result, the signal to noise ratio along a trajectory passing a fold is generally high and consequently the computed $\tilde{F}$ is often not statistically significant, i.e. the probability that the real flux differs from zero is less than 95%.
In other areas where the flux is statistically insignificant, the flux itself is very small.
In the entire domain 90% of the gridpoints in Figure 5 have significant fluxes, 93% have significant dPV/dt and 97% have significant $\partial p/\partial PV$. Similar values are found for the other days.

3.3 Vertical cross-sections of the air mass flux across PV-surfaces

In order to obtain a clearer understanding of the structure of the field of $\tilde{F}$ in tropopause folds, vertical cross-sections of $\tilde{F}$ across these folds have been calculated. Figure 6 shows a cross-section of $\tilde{F}$ (with significance criterion) on 15 April 12 GMT along 40°N, with pressure as the vertical coordinate. A region with large downward fluxes on the eastside of the tropopause trough and a region with smaller upward fluxes in the tropopause ridges west and east of this trough are clearly distinguished. Many insignificant fluxes are found below the 1 PVU surface, where $\partial p/\partial PV$ is very large (generally negative but sometimes positive resulting in a high signal to noise ratio).
In most other tropopause folds (not shown), the region with the largest downward fluxes is also found on the eastside; in some folds this maximum is found in the middle of the fold, but not in the western part. The presence of regions with upward fluxes in tropopause ridges is also found to be a returning feature.

3.4 Area-averaged upward and downward fluxes

As is described in the introduction, the ratio between the upward and downward fluxes should be known in order to calculate the cross-tropopause fluxes of chemical species. To get an impression of this ratio, all upward and downward fluxes (without significance criterion) are added separately and are then averaged over the entire domain (see Table 1). In this calculation, fluxes larger than 0.1 kg m^{-2} s^{-1} and smaller than –0.1 kg m^{-2} s^{-1} are assumed to be non-physical and are set to 0.1 kg m^{-2} s^{-1} and –0.1 kg m^{-2} s^{-1}, respectively. It is striking to see that the ratio R is smallest on April 16, when the strength of the cyclone is maximal, and largest on April 17, when the cyclone has weakened. The ratio between the area averaged upward and downward cross-tropopause fluxes appears to decrease with increasing strength of the cyclone.

TIME	FUP	FDOWN	FNET	R
98041412	1.61E-03	-1.94E-03	-3.35E-04	0.828
98041512	1.36E-03	-1.60E-03	-2.41E-04	0.849
98041612	1.37E-03	-1.89E-03	-5.20E-04	0.725
98041712	1.21E-03	-1.06E-03	1.55E-04	1.147

Table 1: Domain-averaged upward (Fup), downward (Fdown) and net (Fnet) fluxes (in kg m^{-2} s^{-1}) and the ratio of the domain-averaged upward and downward fluxes (R= |Fup/Fdown|) across the 2 PVU surface for 14, 15, 16 and 17 April 1998, 12 GMT.

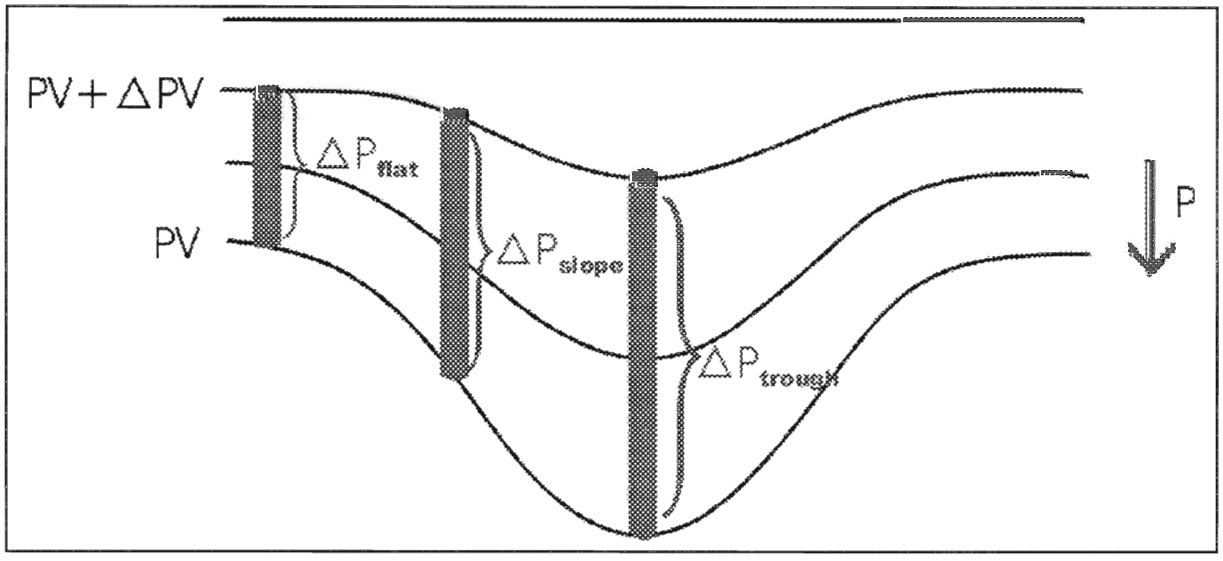

Figure 4: *Illustration of ∂p/∂PV around a tropopause fold. ∂p/∂PV at a sloping tropopause and at a tropopause trough is generally larger than ∂p/∂PV at a flat tropopause.*

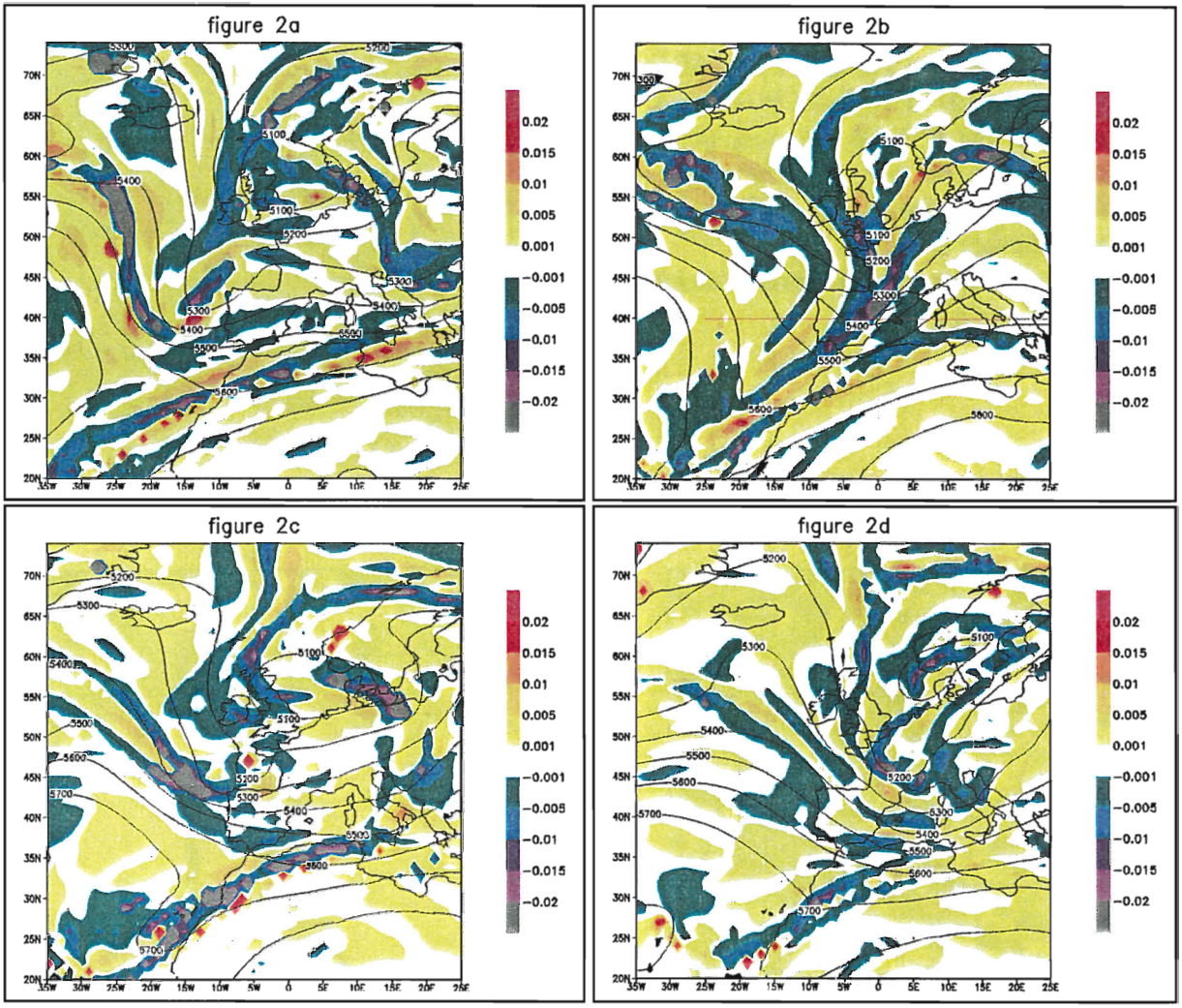

Figure 2: *$\vec{F}$ across the 2 PVU surface (shaded, in kg m^{-2} s^{-1}) together with the 500 hPa geopotential height (contours, in m). Positive values denote transport from the troposphere to the stratosphere. Shown is $\vec{F}$ for (a) 14 April, (b) 15 April, (c) 16 April and (d) 17 April 1998 without significance criterion, all at 12 GMT.*

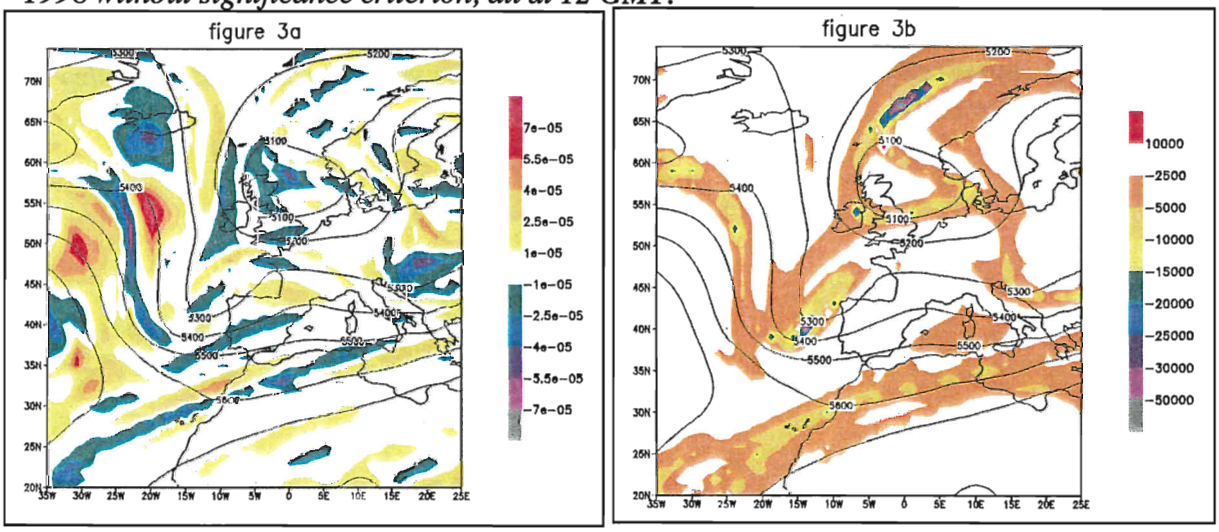

(description Fig. 3 see page 14)

Figure 3: *Decomposition of $\bar{F}$ across the 2 PVU surface on 14 April 12 GMT (as shown in Figure 2a) in dPV/dt (3a, shaded, in PVU s^{-1}) and $\partial p/\partial PV$ (3b, shaded, in Pa PVU^{-1}) together with the 500 hPa geopotential height (contours, in m), both without significance criterion.*
Figure 3c shows the pressure (in hPa) of the 2 PVU surface.

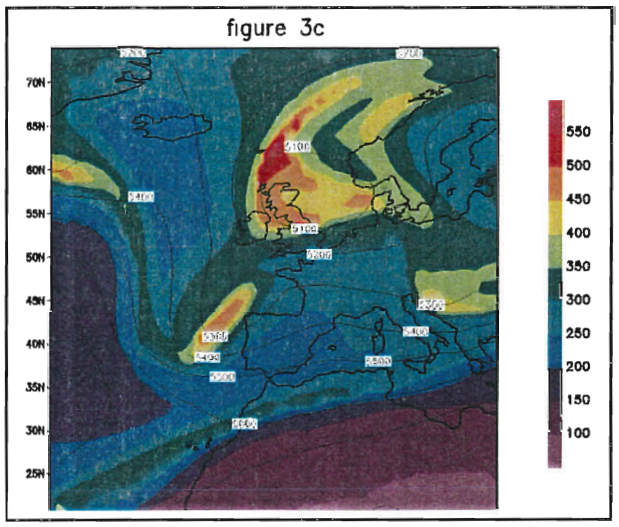

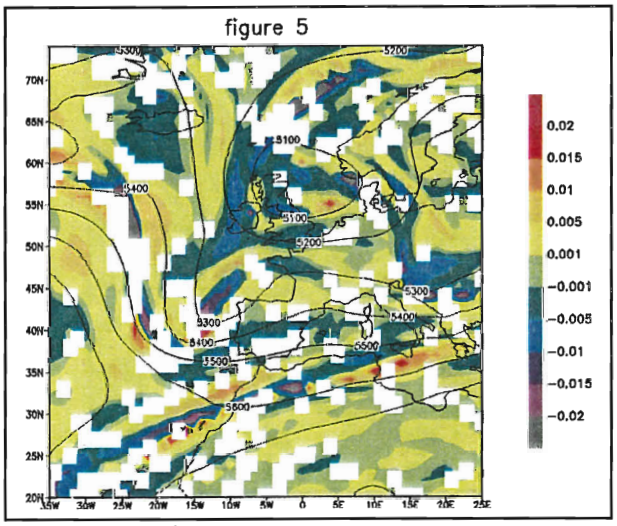

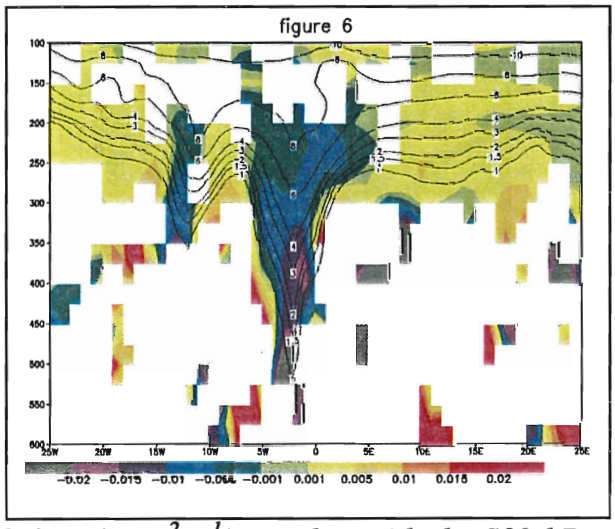

Figure 5: *$\bar{F}$ across the 2 PVU surface (shaded, in kg m^{-2} s^{-1}) together with the 500 hPa geopotential height (contours, in m) on 14 April 12 GMT, with significance criterion. Where $\bar{F}$ is statistically insignificant, the corresponding gridbox has been left blank.*
Figure 6: *Vertical cross-section of $\bar{F}$ (shaded, in kg m^{-2} s^{-1}) on 15 April 12 GMT along 40°N (which is the red line in Figure 2b), with significance criterion (i.e. spaces are left blank where $\bar{F}$ is statistically insignificant), with pressure as the vertical coordinate, together with isolines of PV (in PVU).*

4. Discussion

In this section the parameterization of PV-mixing in the ECMWF-model and the method for calculating the flux across a PV-surface will be discussed. To get an impression of the reliability of the applied method, one should try to judge the reliability of the results, which will be done in section 4.3.

4.1 Parameterization of PV-mixing in the ECMWF-model

As was mentioned in section 2.1.2, a numerical model computes with gridbox mean quantities. In Appendix A it is derived that the PV-change along trajectories computed from gridbox mean circulation data is given by (for simplicity the 2-dimensional situation is considered):

$$\frac{d\overline{PV}}{dt} \equiv \frac{\partial \overline{PV}}{\partial t} + \overline{u}\frac{\partial \overline{PV}}{\partial x} + \overline{v}\frac{\partial \overline{PV}}{\partial y} = -\left[\frac{\partial \overline{u'PV'}}{\partial x} + \frac{\partial \overline{v'PV'}}{\partial y}\right] \quad . \qquad \text{(A3)}$$

The right-hand side of this equation, the divergence of the eddy PV-flux, is a subgrid process, which can not be computed explicitly. Instead, subgrid processes are parameterized in terms of the known gridbox mean quantities. In the ECMWF-model, the eddy ζ (relative vorticity) and the eddy T (temperature) fluxes, i.e. eddy fluxes of quantities that determine the PV rather than the eddy PV-flux itself, are parameterized. The quality of these parameterizations in the ECMWF-model determines the quality of the results of this study.

4.2 Method for calculating the flux across a PV-surface

4.2.1 Calculation of the fluxes

Because of numerical errors due to finite time and space differencing, finding an appropriate method for diagnosing the local and instantaneous flux across a PV-surface is not straightforward. Siegmund *et al.* (1996) have introduced the "advection method", in which the space terms are selectively averaged over time in an Eulerian framework. In this work we have circumvented these time differencing problems by working in a Lagrangian framework. The main problem is that the data suffer from noise. Instant values of *dPV/dt* can therefore be unreliable. To cope with this problem, a certain kind of averaging is necessary. The instant flux in a gridpoint has therefore been computed from data along 6-h forward and backward trajectories starting at the gridpoint.
A second approximation that has been made concerns the calculation of the PV along the trajectories. The gridbox averaged PV, used in numerical atmospheric models, should be calculated according to:

$$\overline{PV} = \overline{\frac{\partial \theta}{\partial p}(\varsigma + f)} = \overline{\frac{\partial \theta}{\partial p}}(\overline{\zeta + f}) + \overline{\left(\frac{\partial \theta}{\partial p}\right)'(\zeta + f)'} \quad , \qquad (10)$$

where the overbar denotes the gridbox mean value and the accent denotes the deviation from that value.
In our calculation of $\overline{PV}$ we were forced to neglect the second term on the right hand side, since the ECMWF-model only provides gridbox mean quantities.

As is described in section 2.2.3, we have made some assumptions to determine whether or not a flux is statistically significant. The different values of $\partial p/\partial PV$ along trajectories are not independent, as we have assumed, so that the real standard deviation is expected to be larger and less gridpoints will have a significant flux.

4.2.2 Averaging period

The averaging period for the calculation of $\bar{F}$ (Eq. 3) has been varied to see how this affects the results. With decreasing period, the reduction of the noise in the results, which was made by averaging, decreases and less values of $\bar{F}$ are statistically significant. As a suitable time period for averaging dPV/dt and $\partial p/\partial PV$, 12 hours is found. Averaging over a longer period does not decrease the noise substantially, but artificially smoothes out the cross-PV fluxes.

4.2.3 Comparison with the Lagrangian flux calculation of Wirth and Egger

As described in the introduction, Wirth and Egger (1999) also used a Lagrangian method to diagnose the cross-tropopause air mass flux. Although the concept of their method is similar to the method applied in this study, there are some noteworthy differences. The similarity is that in both methods a quantity is considered along a trajectory, which is the PV in the present study and the pressure in their study. The pressure difference between the endpoint of a trajectory that started at the tropopause and the tropopause at that endpoint, is then taken by Wirth and Egger as a measure of the cross-tropopause flux.
A difference with our method is that every three hours a reinterpolation of their trajectories to a regular grid is performed in order to avoid a too strong accumulation or dilution of points, which introduces some smoothing. Our method circumvents this problem by calculating forward and backward trajectories starting at a gridpoint and attributing the computed flux to this gridpoint.
A second difference is that Wirth and Egger compute the cross-tropopause flux from information at only the begin and the end of the trajectory, whereas in the present study the averaged PV-rate of change along the trajectory, estimated by a linear least square method, and the trajectory-mean value of $\partial p/\partial PV$ are used to calculate the flux. Our results are, therefore, expected to be less contaminated by noise.

4.3 Results

4.3.1 Large downward fluxes in tropopause folds

As was described in section 3.3 and shown in Figure 5, the largest downward fluxes are found in tropopause folds and at the edge of a more large-scale lowering of the tropopause in the centre of the cyclone. The found maximum in downward fluxes in tropopause folds is expected to be a reliable result for the following reason. A tropopause fold can be looked at as a small-scale lowering of the tropopause. Above a lowered tropopause, the PV is anomalously high. Looking at the definition of PV (Eq. 7a), this would mean an anomalously high positive relative vorticity and an anomalously high $\partial\theta/\partial p$ in this PV-anomaly. The wind speed is therefore highest on both sides of the PV-anomaly, as can be verified from ECMWF-data for April 15 as seen in Figure 7. The wind maxima cause a large shear in the surrounding areas. This wind shear causes strong mixing of air masses in the tropopause fold. Since the PV-gradient is relatively high in this region, this mixing of air masses implies a strong PV-mixing. Comparing Figure 7 with Figure 5, one can clearly see that the PV-mixing is largest

in the regions where the wind shear is maximal. The large downward fluxes found in tropopause folds are therefore thought to be a reliable result, at least in a qualitative sense.
The found tropopause fold along the northwest coast of Africa is thought to lie on a peculiar position. To validate the position of this tropopause fold, GOME (Global Ozone Monitoring Experiment) total ozone columns have been considered (Figure 8). These data show a maximum in the total ozone column, which implies a lowering of the tropopause, virtually along the tropopause fold. The found tropopause fold with its large downward fluxes along the northwest coast of Africa is therefore expected to be a reliable result.

4.3.2 Ratio between downward and upward fluxes

Table 2 shows different values of R (=|Fup/Fdown|) found in different studies with different methods. Before comparing our values with the other values from Table 2, one should realise that R can be strongly case-dependent.
In our results, the largest downward fluxes have been found in tropopause folds. From Table 2 it appears that R decreases if less fluxes outside the tropopause fold are taken into account in the calculation of R.
In Spaete *et al.* (1994) and Lamarque and Hess (1994), R is calculated in a relatively small area around, respectively, a tropopause fold and an extratropical cyclone, whereas in our case, R is calculated averaged over a larger area around an extratropical cyclone. Siegmund *et al.* (1996), finally, computed R for a whole month and for a much larger area.
The domain-averaged upward (Fup) and downward (Fdown) fluxes are comparable to the values found by Lamarque and Hess (1.68×10^{-3} kg m^{-2} s^{-1} and 2.12×10^{-3} kg m^{-2} s^{-1}, respectively) and Spaete et al. (5.79×10^{-3} kg m^{-2} s^{-1} and 2.31×10^{-3} kg m^{-2} s^{-1}, respectively).

Source	R	Averaging period	Averaging area	method	model
Spaete et al. (1994)	0.4	1 day	Area around tropopause fold, travelling with system	Wei-θ across 3 PVU	Mesoscale
Lamarque and Hess (1994)	0.79	4 days	Area around extratropical cyclone travelling with system	Wei-PV across 2 PVU	Mesoscale
Siegmund et al. (1996)	0.97	Month	28°N - 90°N	Wei-p across 3.5 PVU	ECMWF, first guess data
Present study	0.73-1.15	(12 hours)	35°W-25°E 20°N-75°N	Trajectories, Wei-PV across 2 PVU	ECMWF, first guess data

Table 2: Calculations of R (=|Fup/Fdown|) from previous studies and the present study

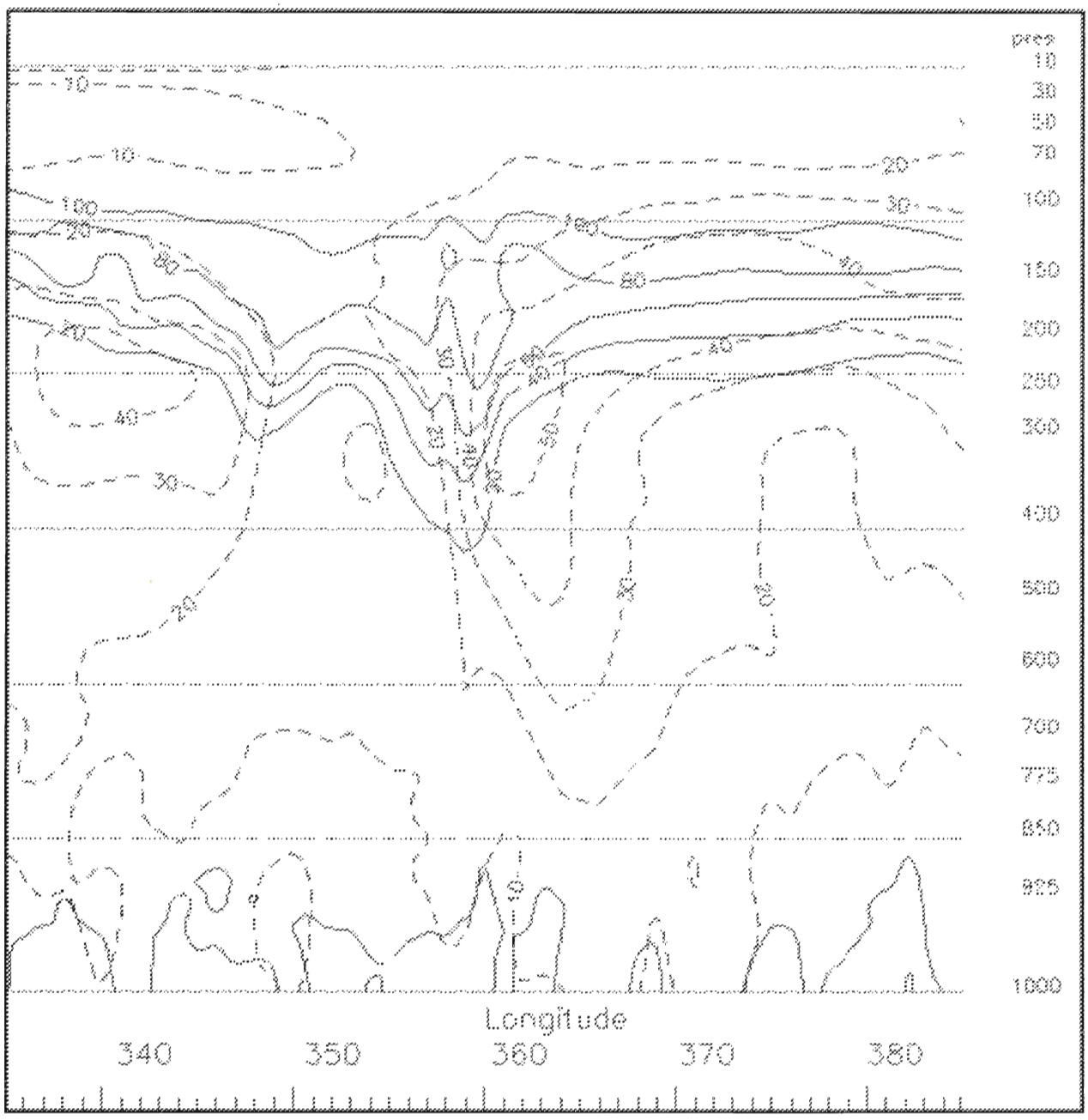

Figure 7: *Vertical cross-section of the wind speed (dotted lines, in m s^{-1}) on 15 April 12 GMT along 40°N (which is the red line in Figure 2b), with pressure as the vertical coordinate (in hPa), together with some isolines of PV (solid lines, in PVU*10).*

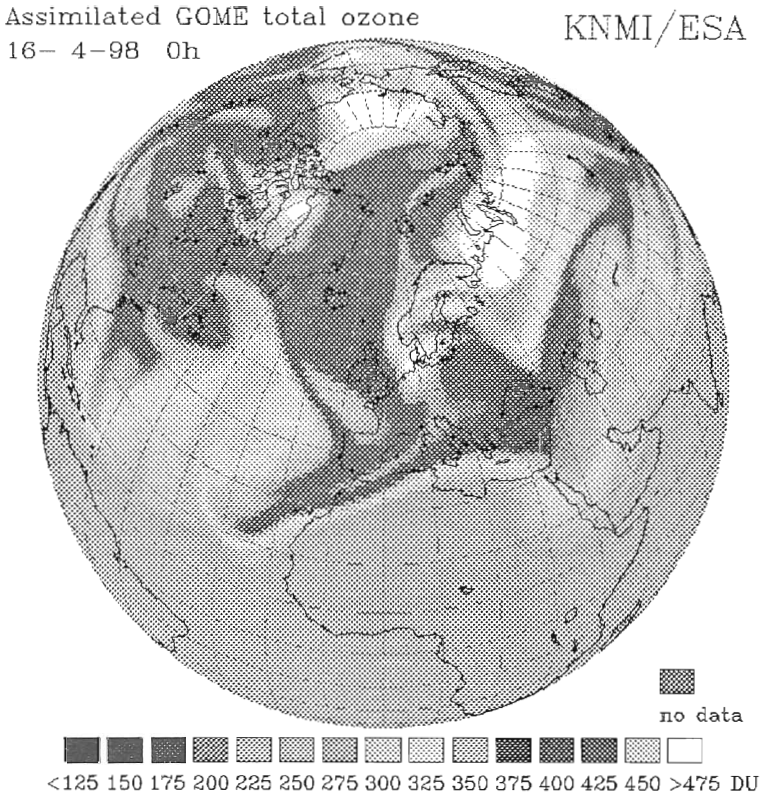

Figure 8: *The GOME total ozone column analysis for 16 April 1998, at 0 GMT*

5. Conclusions

In this work PV-mixing is investigated. Since the air mass flux across PV-surfaces appears to us physically more interesting than the distribution of the PV-change, the fluxes across PV-surfaces rather than the PV-change due to PV-mixing have been investigated.
A new Lagrangian method for diagnosing the air mass flux across PV-surfaces, in particular across the tropopause, is introduced. The flux is computed from the PV and $\partial p/\partial PV$ along 12-h trajectories that pass the gridpoint for which the flux is estimated. The trajectories are computed from ECMWF circulation data. In the extratropical cyclone to which the method has been applied, the PV-change due to diabatic heating gradients is found to be negligible compared to the PV-change due to mixing. The error in the flux across PV-surfaces (the "noise") is quantified and used to determine the statistical significance of the flux.
The computed field of the air mass flux across PV-surfaces is dominated by elongated patterns of statistically significant large downward and small upward fluxes. The downward fluxes mainly occur in regions of a tropopause fold, whereas the upward fluxes are found near tropopause ridges. The area-averaged upward (Fup) and downward (Fdown) fluxes, which both lie between 1 and 2×10^{-3} kg m^{-2} s^{-1}, are comparable to the values found by previous studies. The ratio between the area averaged upward and downward cross-tropopause fluxes appears to decrease with increasing strength of the cyclone.
The results are thought to be reliable, at least in a qualitative sense, because the largest downward fluxes in the tropopause fold occur in regions with maximum wind shear. The geographical agreement between tropopause folds with large downward fluxes and the high total ozone values is good. Although several approximations have been made in the applied new Lagrangian method, this method appears to be an appropriate tool for diagnosing PV-mixing in general and stratosphere-troposphere exchange in particular.

APPENDIX A: Mathematical consideration of PV-mixing

In a gridbox fixed in space, the change in the gridbox-mean PV, $\partial\overline{PV}/\partial t$, is determined by the difference between the in- and outgoing fluxes of PV. This can be expressed, in a 2-dimensional situation, as:

$$\frac{\partial\overline{PV}}{\partial t} = -\left[\frac{\partial\overline{uPV}}{\partial x} + \frac{\partial\overline{vPV}}{\partial y}\right] \quad . \qquad (A1)$$

Writing u, v and PV as $u = \bar{u} + u'$, $v = \bar{v} + v'$ and $PV = \overline{PV} + PV'$, where the overbar denotes mean values at the in- or outgoing side of the gridbox, Eq. (A1) can be written as:

$$\frac{\partial\overline{PV}}{\partial t} = -\left[\frac{\partial\bar{u}\overline{PV}}{\partial x} + \frac{\partial\bar{v}\overline{PV}}{\partial y} + \frac{\partial\overline{u'PV'}}{\partial x} + \frac{\partial\overline{v'PV'}}{\partial y}\right] \quad . \qquad (A2)$$

Applying the continuity equation, Eq. (A2) can be written as:

$$\frac{d\overline{PV}}{dt} \equiv \frac{\partial\overline{PV}}{\partial t} + \bar{u}\frac{\partial\overline{PV}}{\partial x} + \bar{v}\frac{\partial\overline{PV}}{\partial y} = -\left[\frac{\partial\overline{u'PV'}}{\partial x} + \frac{\partial\overline{v'PV'}}{\partial y}\right] \quad . \qquad (A3)$$

The PV-change along trajectories computed from gridbox mean circulation data should be interpreted as $d\overline{PV}/dt$ and therefore depends on the eddy PV-flux divergence.

APPENDIX B: Further investigation of the noise

Investigating the PV along trajectories calculated with circulation data from ECMWF-analyses more thoroughly, a 6-h fluctuation is found, which is most obvious in areas where the PV-gradient is largest. Since this 6-h fluctuation is not expected to be a physical fluctuation, it is considered as noise. This noise is likely caused by interpolation errors and errors in the ECMWF-data.

Since the temporal resolution of the ECMWF-data is also 6 hours, errors in the ECMWF-data are suspected to be a cause of the fluctuations. Moreover, in a run with a 12-h data resolution, the amplitude as well as the period of the fluctuations doubled. It was therefore suspected that the analysed datafields are affected by input of new measurements every 6 hours (in this case) in such a way that non-physical fluctuations of the PV are generated in a run with analysis data. Forecast data are used to test this hypothesis.

In the forecast run the fluctuations vanished for only a small part. The 6-h fluctuations are therefore only for a small part caused by the input of new measurements every 6 hours. Errors due to interpolation by the trajectory model are expected to be the main cause of the 6-h fluctuations.

Since the Tracer Conservation Error was smaller in the forecast run than in the analysis run, the PV is better conserved in the forecast run than in the run with analysis data. Since consequently the noise is smaller in the forecast run, we used forecast data rather than analysis data to calculate $\tilde{F}$.

References

Brewer A.M., 1949, Evidence for a world circulation provided by the measurements of helium and water vapour distribution in the stratosphere, *Q.J.R. Meteorol. Soc.* **75**, 351-363.

Dobson G.M.B., 1956, Origin and distribution of polyatomic molecules in the atmosphere, *Proc. Roy. Meteor. Soc.* **A236**, 187-193.

Gettelman A. and Sobel A.H., 1998, Direct diagnoses of Stratospher-Troposphere Exchange, *accepted to The Journal of Atmospheric Sciences.*

Hoerling M.P., Schaack T.K. and Lenzen A.J., 1993, A global analysis of stratospheric-tropospheric exchange during northern winter, *Mon. Weather Rev.* **121**, 162-172.

Holton, J.R., Haynes, P.H., McIntyre, M.E., Douglass, A.R., Rood, R.B. and Pfister, L., 1995, Stratosphere-troposphere exchange, *Rev. Geophys.*, **33**, 403-439.

Hoskins, B.J., McIntyre, M.E. and Robertson, A.W., 1985, On the use and significance of isentropic potential vorticity maps, *Q.J.R. Meteorol. Soc.,* **111**, 877-946.

IPCC (Intergovernmental Panel on Climate Change), 1999, special report on 'Aviation and the global atmosphere', Cambridge University Press.

Lamarque, J. and Hess, P.G., 1994, Cross-Tropopause Mass Exchange and Potential Vorticity Budget in a Simulated Tropopause Folding, *J. Atmos. Sci.*, **51**, 2246-2269.

Lyttkens E., 1963, Standard Errors of Regression Coefficients in the Case of Autocorrelated Residuals, from: 'Time Series Analysis', edited by M. Rosenblatt, John Wiley and Sons, Inc., p. 38-60.

Petterssen, S., 1940, Weather Analysis and Forecasting. McGraw-Hill, p. 221-223.

Scheele, M.P., Siegmund P.C., and Velthoven van P.F.J., 1996, Sensitivity of trajectories to data resolution and its dependence on the starting point: in or outside a tropopause fold, *Meteorol. Appl. 3*, 267-273.

Shapiro, M.A., 1980, Turbulent Mixing within Tropopause Folds as a Mechanism for the Exchange of Chemical Constituents between the Stratosphere and Troposphere, *J. Atmos. Sci.*, **37**, 994-1004.

Siegmund, P.C., Velthoven van P.F.J. and Kelder H., 1996, Cross-tropopause transport in the extratropical northern winter hemisphere, diagnosed from high-resolution ECMWF data, *Q.J.R. Met. Soc.*, **122**, 1921-1941.

Spaete, P., 1994, Stratospheric-Tropospheric Mass Exchange during the Presidents' Day Storm, *Monthly Weather Review*, **122**, 424-439.

Stohl A. and Seibert P., 1998, Accuracy of trajectories as determined from the conservation of meteorological tracers, *Q.J.R. Meteorol. Soc.*, 1465-1484.

Stohl, A., Wotawa, G., Seibert, P. and Kromp-Kolb, H., 1995, Interpolation errors in wind fields as a function of spatial and temporal resolution and their impact on different types of kinematic trajectories, *J. Appl. Meteorol.*, **35**: 2149-2165.

Wernli H. and Davies H.C., 1997, A lagrangian-based analysis of extratropical cyclones. I: The method and some applications, *Q.J.R.Meteorol. Soc.*, **123**, 467-489.

Wirth, V. and Egger J., 1999, Diagnosing Extratropical Synoptic-Scale Stratosphere-Troposphere Exchange: A Case Study, *Q.J.R. Meteorol. Soc.*, **125**, 635-655.

WMO, 1995, 'Scientific assessment of ozone depletion: 1994'. Global ozone research and monitoring project, Report No. 37 World Meteorological Organization, Geneva, Switzerland.

KNMI-PUBLICATIES, VERSCHENEN SEDERT 1995

Een overzicht van eerder verschenen publicaties, wordt verzoek toegezonden door de Bibliotheek van het KNMI, postbus 201, 3730 AE De Bilt, tel. 030 - 2 206 855, fax. 030 - 2 210 407; e-mail: biblioth@knmi.nl

▼ KNMI-PUBLICATIE MET NUMMER

150-28 Sneeuwdek in Nederland 1961-1990 / A.M.G. Klein Tank
180a List of acronyms in environmental sciences : revised edition / [compiled by P. Geerders and M. Waterborg]
181b FM12 SYNOP internationale en nationale regelgeving voor het coderen van de groepen 7wwW1W2 en 960ww; derde druk
183-1 Rainfall in New Guinea (Irian Jaya) / T.B. Ridder
183-2 Vergelijking van zware regens te Hollandia (Nieuw Guinea), thans Jayapura (Irian Jaya) met zware regens te De Bilt / T. B. Ridder
183-3 Verdamping in Nieuw-Guinea, vergelijking van gemeten hoeveelheden met berekende hoeveelheden / T.B. Ridder
183-4 Beschrijving van het klimaat te Merauke, Nieuw Guinea, in verband met de eventuele vestiging van een zoutwinningsbedrijf / T.B. Ridder a.o.
183-5 Overzicht van klimatologische en geofysische publikaties betreffende Nieuw-Guinea / T.B. Ridder
184a Inleiding tot de algemene meteorologie : studie-uitgave ; 2e druk / B. Zwart, A. Steenhuisen, m.m.v. H.J. Krijnen
185a Handleiding voor het gebruik van sectie 2 van de FM 13-X SHIP-code voor waarnemers op zee / KNMI, KLu; KM
186-I Rainfall generator for the Rhine Basin: single-site generation of weather variables by nearest-neighbour resampling / T. Brandsma a.o.
187 De wind in de rug: KNMI-weerman schaatst de Elfstedentocht / H. van Dorp
188 SODA workshop on chemical data assimilation: proceedings; 9-10 December 1998, KNMI, De Bilt, The Netherlands

▼ TECHNISCH RAPPORT = TECHNICAL REPORT (TR)

170 DARR-94 / C.P.G. Lomme
171 EFEDA-91: documentation of measurements obtained by KNMI / W.A.A. Monna a.o.
172 Cloud lidar research at the Royal Netherlands Meteorological Institute KNMI2B2, version 2 cloud lidar analysis / A.Y. Fong a.o.
173 Measurement of the structure parameter of vertical wind-velocity in the atmospheric boundary layer / R. van der Ploeg
174 Report of the ASGASEX'94 workshop / ed. by W.A. Oost
175 Over slecht zicht, bewolking, windstoten en gladheid / J. Terpstra
176 Verification of the WAQUA/CSM-16 model for the winters 1992-93 and 1993-94 / J.W. de Vries
177 Nauwkeuriger nettostraling meten / M.K. van der Molen en W. Kohsiek
178 Neerslag in het stroomgebied van de Maas in januari 1995: waarnemingen en verificatie van modelprognoses / R.Jilderda a.o.
179 First field experience with 600PA phased array sodar / H. Klein Baltink
180 Een Kalman-correctieschema voor de wegdektemperatuurverwachtingen van het VAISALA-model / A. Jacobs
181 Calibration study of the K-Gill propeller vane / Marcel Bottema
182 Ontwikkeling van een spectraal UV-meetinstrument / Frank Helderman
183 Rainfall generator for the Rhine catchment : a feasibility study / T. Adri Buishand and Theo Brandsma
184 Parametrisatie van mooi-weer cumulus / M.C. van Zanten
185 Interim report on the KNMI contributions to the second phase of the AERO-project / Wiel Wauben, Paul Fortuin a.o.
186 Seismische analyse van de aardbevingen bij Middelstum (30 juli 1994) en Annen (16 augustus '94 en 31 januari '95) / [SO]
187 Analyse wenselijkheid overname RIVM-windmeetlokaties door KNMI / H. Benschop
188 Windsnelheidsmetingen op zeestations en kuststations: herleiding waarden windsnelheden naar 10-meter niveau / H. Benschop
189 On the KNMI calibration of net radiometers / W. Kohsiek
190 NEDWAM statistics over the period October 1994 - April 1995 / F.B. Koek
191 Description and verification of the HIRLAM trajectory model / E. de Bruijn
192 Tiltmeting . een alternatief voor waterpassing ? / H.W. Haak
193 Error modelling of scatterometer, in-situ and ECMWF model winds; a calibration refinement / Ad Stoffelen
194 KNMI contribution to the European project POPSICLE / Theo Brandsma a.o.
195 ECBILT a coupled atmosphere ocean sea-ice model for climate predictability studies / R.J. Haarsma a.o.
196 Environmental and climatic consequences of aviation: final report of the KNMI contributions to the AERO-project / W. Wauben a.o.
197 Global radiation measurements in the operational KNMI meteorological network: effects of pollution and ventilation / F. Kuik
198 KALCORR: a kalman-correction model for real-time road surface temperature forecasting / A. Jacobs
199 Macroseismische waarnemingen Roswinkel 19-2-1997 / B. Dost e.a.
200 Operationele UV-metingen bij het KNMI / F. Kuik
201 Vergelijking van de Vaisala's HMP233 en HMP243 relatieve luchtvochtigheidsmeters / F. Kuik
202 Statistical guidance for the North Sea / Janet Wijngaard and Kees Kok
203 UV-intercomparison SUSPEN / Foeke Kuik and Wiel Wauben
204 Temperature corrections on radiation measurements using Modtran 3 / D.A. Bunskoek, A.C.A.P. van Lammeren and A.J. Feijt
205 Seismisch risico in Noord-Nederland / Th. De Crook, H.W. Haak en B. Dost
206 The HIRLAM-STAT-archive and its application programs / Albert Jacobs
207 Retrieval of aerosol properties from multispectral direct sun measurements / O.P. Hasekamp
208 The KNMI Garderen Experiment, micro-meteorological observations 1988-1989; instruments and data / F.C. Bosveld a.o.
209 CO2 in water and air during ASGAMAGE: concentration measurements and consensus data / Cor M.J. Jacobs, Gerard J. Kunz, Detlev Sprung a.o.
210 Elf jaar Cabauw-metingen / J.G. van der Vliet
211 Indices die de variabiliteit en de extremen van het klimaat beschrijven / E.J. Klok
212 First guess TAF-FGTAF: semi-automation in TAF production / Albert Jacobs
213 Zeer korte termijn bewolkingsverwachting met behulp van METCAST: een verificatie en beschrijving model-uitvoer / S.H. van der Veen
214 The implementation of two mixed-layer schemes in the HOPE ocean general circulation model / M. van Eijk
215 Stratosphere-troposphere exchange of ozone, diagnosed from an ECMWF ozone simulation experiment / Harm Luykx
216 Evaluatierapport Automatisering Visuele Waarnemingen Ontwikkeling Meestsystemen / Wiel Wauben en Hans de Jongh
217 Verificatie TAF en TREND / Hans van Bruggen
218 LEO - LSG and ECBILT coupled through OASIS: description and manual/A. Sterl
219 [nog niet verschenen]
220 Back-up modellering van windmeetmasten op luchthavens / Ilja Smits

▼ WETENSCHAPPELIJK RAPPORT = SCIENTIFIC REPORT (WR)

95-02 Internal variability of the ocean generated by a stochastic forcing / M.H.B. van Noordenburg
95-03 Applicability of weakly nonlinear theory for the planetary-scale flow / E.A. Kartashova
95-04 Changes in tropospheric NOx and O3 due to subsonic aircraft emissions / W.M.F. Wauben a.o.
95-05 Numerical studies on the Lorenz84 atmosphere model / L. Anastassiades
95-06 Regionalisation of meteorological parameters / W.C. de Rooy
95-07 Validation of the surface parametrization of HIRLAM using surface-based measurements and remote sensing data / A.F. Moene a.o.
95-08 Probabilities of climatic change : a pilot study / Wieger Fransen (ed.) a.o.
96-01 A new algorithm for total ozone retrieval from direct sun measurements with a filter instrument / W.M.F. Wauben
96-02 Chaos and coupling: a coupled atmosphere ocean-boxmodel for coupled behaviour studies / G. Zondervan
96-03 An acoustical array for subsonic signals / H.W. Haak
96-04 Transformation of wind in the coastal zone / V.N. Kudryavtsev a.o.
96-05 Simulations of the response of the ocean waves in the North Atlantic and North Sea to CO2 doubling in the atmosphere / K. Rider a.o.
96-06 Microbarograph systems for the infrasonic detection of nuclear explosions / H.W. Haak and G.J. de Wilde
96-07 An ozone climatology based on ozonesonde measurements / J.P.F. Fortuin
96-08 GOME validation at KNMI and collaborating institutes / ed. P Stammes a.o.
97-01 The adjoint of the WAM model / H. Hersbach
97-02 Optimal interpolation of partitions: a data assimilation scheme for NEDWAM-4; description and evaluation of the period November 1995 - October 1996 / A.Voorrips
97-03 SATVIEW: a semi-physical scatterometer algorithm / J.A.M. Janssen a.o.
97-04 GPS water vapour meteorology status report / H. Derks a.o.
97-05 Climatological spinup of the ECBILT oceanmodel / Arie Kattenberg a.o.
97-06 Direct determination of the air-sea transfer velocity of CO2 during ASGAMAGE / J.C.M. Jacobs, W. Kohsiek and W.A. Oost
97-07 Scattering matrices of ice crystals / M. Hess, P. Stammes a.o.
97-08 Experiments with horizontal diffusion and advection in a nested fine mesh mesoscale model / E.I.F. de Bruijn
97-09 On the assimilation of ozone into an atmospheric model / E.Valur Hólm
98-01 Steady state analysis of a coupled atmosphere ocean-boxmodel / F.A. Bakker
98-02 The ASGAMAGE workshop, September 22-25, 1997 / ed. W.A. Oost
98-03 Experimenting with a similarity measure for atmospheric flows / R.A. Pasmanter and X.-L. Wang
98-04 Evaluation of a radio interferometry lightning positioning system / H.R.A. Wessels
98-05 Literature study of climate effects of contrails caused by aircraft emissions / V.E. Pultau
99-01 Enhancement of solar and ultraviolet surface irradiance under partial cloudy conditions / Serdal Tunç
99-02 Turbulent air flow over sea waves: simplified model for applications / V.N. Kudryavtsev, V.K. Makin and J.F. Meirink
99-03 The KNMI Garderen experiment, micro-meteorological observations 1988-1989: corrections / Fred C. Bosveld
99-04 ASGAMAGE: the ASGASEX MAGE experiment . final report / ed. W.A.Oost